Spinocerebellar ataxia type 11-associated alleles of *Ttbk2* dominantly interfere with ciliogenesis and cilium stability.

Emily Bowie[1,2], Ryan Norris[3], and Kathryn V. Anderson[3], and Sarah C. Goetz*[1,2]

[1]Department of Pharmacology and Cancer Biology, Duke University School of Medicine, Durham, NC 27701, USA
[2]University Program in Genetics and Genomics, Duke University, Durham, NC 27701, USA
[3]Developmental Biology Program, Sloan Kettering Institute, New York, NY 10021, USA.

*Author for correspondence: sarah.c.goetz@duke.edu

Abstract

Spinocerebellar ataxia type 11 (SCA11) is a rare, dominantly inherited human ataxia characterized by atrophy of Purkinje neurons in the cerebellum. SCA11 is caused by mutations in the gene encoding the serine threonine kinase Tau tubulin kinase 2 (TTBK2) that result in premature truncations of the protein. We previously showed that TTBK2 is a key regulator of tha assembly of primary cilia *in vivo*. In this work, we present evidence that SCA11-associated mutations are dominant negative alleles and that the resulting truncated protein ($TTBK2^{SCA11}$) interferes with full length TTBK2 in ciliogenesis. A *Ttbk2* allelic series revealed that upon partial reduction of full length TTBK2 function, $TTBK2^{SCA11}$ can interfere with the activity of the residual wild-type protein to decrease cilia number and interrupt cilia-dependent Sonic hedgehog (SHH) signaling. Our studies have also revealed new functions for TTBK2 after cilia initiation in the control of cilia length, SMO trafficking, and cilia stability. The studies provide a molecular foundation to understand the cellular and molecular pathogenesis of human SCA11, and help account for the link between ciliary dysfunction and neurodegenerative diseases.

Introduction

Primary cilia play a critical role in many aspects of embryonic development. Cilia are important for the development of the brain and central nervous system, which accounts for the structural brain defects, cognitive impairments and other neurological disorders that are characteristic of many human ciliopathies(1–3). Cilia are present on a wide variety of neurons and astroglia within the adult brain, although the specific requirements for these organelles in the function of the adult brain are not well understood.

In prior work, we identified a serine-threonine kinase, TTBK2, that is essential for initiating the assembly of primary cilia in the embryo(4). In addition to the critical requirement for TTBK2 in ciliogenesis, particular dominant mutations that disrupt TTBK2 cause a hereditary ataxia, spinocerebellar ataxia type 11 (SCA11)(5). Like other subtypes of SCA, SCA11 is a

progressive neurodegenerative condition predominantly affecting the cerebellum. At the cellular level, SCA11 is characterized by cerebellar atrophy resulting from a degeneration of Purkinje cells (PCs) of the cerebellum. However, the molecular basis underlying this pathology as well as for the dominant mode of SCA11 inheritance remain unknown. Three different familial *SCA11* mutations in *TTBK2* that cause late-onset ataxia are associated with insertions or deletions of one or two bases that cause frame shifts and produce similar truncations of TTBK2 protein at approximately AA 450(5, 6). A fourth mutation in *TTBK2* that causes an earlier-onset disease truncates the protein at AA 402(7).

Because TTBK2 is essential for the biogenesis of primary cilia, which are in turn essential for the development of the nervous system, we hypothesize that the SCA11-associated mutations disrupt the function of TTBK2 in cilia formation. In previous structure-function experiments, we tested the ability of truncations of TTBK2 to restore cilia in *Ttbk2* null mutant cells and found that truncations of TTBK2 corresponding with the SCA11-associated mutations were unable to rescue cilia formation. We also found that, when expressed in WT cells, these truncations also partially suppress cilia formation(4), suggesting the SCA11-associated truncations may act by interfering with the activity of the wild-type gene product.

Here, we examine phenotypes of mice with *Sca11*-like truncating mutations knocked into the endogenous *Ttbk2* locus. We find that *Ttbk2*^{sca11} homozygotes are indistinguishable from the null allele: cilia initiation fails and cilia-dependent SHH signaling is blocked. Using a series of different *Ttbk2* alleles, we show that SCA11-associated truncated proteins interfere with the function of full-length TTBK2 in cilium assembly. In addition, these allelic combinations have uncovered a previously unappreciated function for TTBK2 in the regulation of cilia stability. TTBK2 is localized to the mother centriole in un-ciliated cells and it at the transition zone of the cilium. In this study, we present evidence from hypomorphic allelic combinations that TTBK2 also acts after cilium initiation to regulate cilium stability, in part by countering a cilium disassembly pathway.

Results

Embryos homozygous for a familial SCA11-associated mutation in Ttbk2 phenocopy Ttbk2 null embryos.

To examine the effects of SCA11-associated TTBK2 truncations on the function of the protein in cilia, we used an allele of *Ttbk2* in which a mutation precisely recapitulating one of the human SCA11-causing mutations was knocked into the mouse *Ttbk2* genomic locus(8). *Ttbk2*$^{sca11/sca11}$ homozygous embryos were previously reported to die by E11, but their developmental and cellular phenotypes were not described. We found that E10.5 *Ttbk2*$^{sca11/sca11}$ embryos exhibit morphological phenotypes that are strikingly similar to those that we previously described in embryos homozygous for an ENU-induced null allele of *Ttbk2*, *Ttbk2*$^{bby/bby(4)}$ (referred to from this point as *Ttbk2*$^{null/null}$) , including holoprosencephaly, a pointed midbrain flexure, and randomized heart laterality (Figure 1A). Also similar to *Ttbk2*$^{null/null}$, embryos, the *Ttbk2*$^{sca11/sca11}$ embryos exhibited neural patterning defects consistent with a failure to respond to SHH, including the absence of the NKX2.2+ V3 interneuron progenitors that require high levels of SHH activity (Figure 1C, F) and reduced numbers of ISL1+ motor neurons, which are shifted ventrally to the ventral midline (Figure 1B, E).

Ttbk2$^{sca11/sca11}$ embryos lacked cilia in mesenchymal cells surrounding the neural tube (Figure 1F, I) as well as the limb buds and neural tube (data not shown), as assayed by immunostaining for the ciliary membrane protein ARL13B. Mouse embryo fibroblasts (MEFs) derived from *Ttbk2*$^{sca11/sca11}$ embryos failed to recruit IFT proteins to the basal body and retained the cilium-suppressing centrosomal protein CP110 at the distal mother centriole (Figure S1), as originally reported for the *Ttbk2*$^{null/null}$ allele(4), showing that the truncated TTBK2 protein produced by the SCA11-associated mutation is unable to function in cilia formation. The truncated TTBK2 protein produced by the SCA11-associated mutations can be detected in heterozygous knockin animals(8), but is unable to promote cilium formation. As SCA11 is a late

adult-onset phenotype seen in in *SCA11*/+ individuals, we examined the phenotype of adult *Ttbk2*$^{scall/+}$ mice. At 3 months of age, the cerebellar architecture of the *Ttbk2*$^{scall/+}$ animals was not distinguishable from that of wild type (Figure S2).

Decreased rescue of Ttbk2$^{sca11/sca11}$ *MEFs by TTBK2-GFP*

SCA11 is dominantly inherited: affected patients are heterozygous for the mutation and have one wild-type allele(5). We previously found that overexpression of TTBK2^{SCA11} in WT fibroblasts had a modest but significant cilia-suppression activity(4), leading us to propose that *Ttbk2*^{sca11} may be a dominant-negative (antimorphic) allele of *Ttbk2*. To further test this hypothesis, we expressed WT TTBK2-GFP in MEFs derived from both *Ttbk2*$^{null/null}$ and *Ttbk2*$^{sca11/sca11}$ embryos using the same retroviral transduction system we previously employed for rescue experiments, and compared the ability of WT TTBK2 to rescue cilia formation in cells of these two genotypes. The frequency of rescue of cilia in *Ttbk2*$^{sca11/sca11}$ MEFs was approximately half of what that in *Ttbk2*$^{null/null}$ MEFs, in which ciliogenesis was fully rescued (34.1 4.6% vs 66.2 +/-3.3%; p= 0.0002; Figure 2A, B). The intensity of ARL13B was also reduced in cilia of *Ttbk2*$^{sca11/sca11}$ MEFs expressing TTBK2-GFP compared to cilia in *Ttbk2*$^{null/null}$ MEFs (WT: 120.4 +/- 4.96 A.U., *Ttbk2*$^{bby/bby}$+ TTBK2-GFP: 103.2 +/- 3.37 A.U., *Ttbk2*$^{sca11/sca11}$+ TTBK2-GFP: 58.93 +/- 6.14 A.U.; Figure 2C, D), although the cilia did not differ significantly in length (WT: 3.468 +/- 0.154, *Ttbk2*$^{bby/bby}$+ TTBK2-GFP: 2.874 +/- 0.074, *Ttbk2*$^{sca11/sca11}$+ TTBK2-GFP: 3.438 +/- 0.194,Figure 2C, E). Together, these results suggest that the ability of exogenous TTBK2-GFP to restore cilia in mutant fibroblasts is inhibited by the presence of the truncated TTBK2^{SCA11} protein in these cells.

Ttbk2^{sca11} *acts as an antimorphic allele*

To test whether TTBK2^{SCA11} dominantly interferes with WT TTBK2 function *in vivo*, we took advantage of a *Ttbk2* allelic series. We generated mice that carry a gene trap allele of

Ttbk2 (*Ttbk2*$^{tm1a(EUCOMM)Hmgu}$) from ES cells obtained from the European Mutant Mouse Cell Repository (EuMMCR). Although the targeting strategy was designed to trap splicing of an early *Ttbk2* exon (Figure S3A), the homozygous gene trap mice (*Ttbk2*$^{gt/gt}$) were viable past weaning, developing variably penetrant hydrocephalus (Figure S3B, E) and polycystic kidneys by 6 months of age (Figure S3E). Transcript analysis showed that this allele produced mRNAs with the predicted gene trap transcript and a wild-type RNA formed by splicing around the gene trap insertion (Figure S3C). Consistent with these animals producing some WT protein product, by Western blot we detected a small amount of TTBK2 protein, running at the same molecular weight as WT TTBK2 (Figure S3E). We conclude that *Ttbk2*^{gt} is a partial loss-of-function (hypomorphic) allele that produces a reduced amount of wild-type, full-length TTBK2 protein.

Consistent with the hypomorphic character of the gene trap allele, *Ttbk2*$^{gt/null}$ embryos had a phenotype intermediate between that of *Ttbk2*$^{null/null}$ and the *Ttbk2*$^{gt/gt}$ homozygotes: *Ttbk2*$^{null/gt}$ embryos and neonates were recovered at nearly Mendelian frequencies up to birth (P0) but died by P1. At E15.5, in contrast to *Ttbk2*$^{gt/gt}$ embryos, which showed wild-type morphology, *Ttbk2*$^{null/gt}$ embryos had fully penetrant polydactyly on all 4 limbs, consistent with a disruption in Hh-dependent limb patterning (Figure 3A-C).

We reasoned that the *Ttbk2*^{gt} allele, with lowered levels of TTBK2 protein, might provide a sensitized genetic background to better compare the effects of the *Ttbk2*^{null} and *Ttbk2*^{sca11} alleles. *Ttbk2*$^{sca11/gt}$ embryos showed similar overall morphology to *Ttbk2*$^{null/gt}$ embryos at E15.5, with fully penetrant polydactyly on all 4 limbs. While some *Ttbk2*$^{sca11/gt}$ neonates could be recovered at P0, they were present at a sub-Mendelian frequency: only 9% of pups recovered at birth from *Ttbk2*$^{gt/+}$ x *Ttbk2*$^{sca11/+}$ crosses genotyped as *Ttbk2*$^{sca11/gt}$ (Table S1), suggesting some prenatal lethality.

We compared ventral neural patterning in *Ttbk2*$^{gt/gt}$, *Ttbk2*$^{null/gt}$, and *Ttbk2*$^{sca11/gt}$ embryos to determine whether *Ttbk2*$^{sca11/gt}$ embryos had more severe disruption of SHH signaling than seen in *Ttbk2*$^{null/gt}$ embryos. We found that neural patterning in E10.5 *Ttbk2*$^{gt/gt}$

embryos was similar to that in *Ttbk2*$^{gt/+}$ embryos (Figure 3 E-F, I-J), and *Ttbk2*$^{null/gt}$ embryos exhibited quite mild defects in neural patterning, with a normal motor neuron (ISL1) domain, and a slight ventral shift in the domain of NKX2.2 expression (Figure 3G, K). In contrast, the ISL1+ motor neuron domain was shifted ventrally in *Ttbk2*$^{sca11/gt}$ embryos and spanned the ventral midline (Figure 3H), and there was extensive intermixing of OLIG2+ and NKX2.2+ progenitor populations (Figure 3L), consistent with a more severe disruption in SHH-dependent patterning. This enhanced SHH patterning phenotype, combined with the increase in embryonic lethality of the *Ttbk2*$^{sca11/gt}$ animals, provides genetic support for *Ttbk2*^{sca11} as a dominant negative allele.

TTBK2^{SCA11} *does not physically interact with full length TTBK2*

To investigate how the truncated SCA11-associated protein interferes with the function of WT TTBK2, we tested whether TTBK2^{SCA11} could physically interact with full length TTBK2. Previous studies have found that TTBK2 molecules physically associate and that TTBK2 can phosphorylate its own C terminus(9), suggesting that like other members of the CK1 family(10), TTBK2 may form a homodimer, and this association could have regulatory significance. We therefore tested the ability of different fragments of TTBK2 to interact with full length TTBK2 by co-immunoprecipitation. Consistent with previous reports, V5-tagged full length TTBK2 co-precipitates with full length TTBK2-GFP when both constructs are expressed in HEK293T cells (Figure 4B). Full length TTBK2-V5 also co-precipitates with the C terminus of TTBK2 (TTBK2$^{306-1243}$-GFP), but not with the N-terminal domain of TTBK2 (TTBK2$^{1-306}$) (which includes the kinase domain), nor with a SCA11-associated TTBK2 truncation (TTBK2$^{1-443}$) (Figure 4C). Thus, the C-terminus of TTBK2 (amino acids 450-1243) is essential for this self-interaction. Consistent with this finding, TTBK2^{SCA11}-V5 is also unable to co-immunoprecipitate with TTBK2^{SCA11}-GFP. Lacking the C-terminus, TTBK2^{SCA11} is therefore no longer able to form a dimer either with itself or with full length TTBK2. The loss of these interactions has implications for the regulation of TTBK2^{SCA11} as well as its interactions with substrates. As the SCA11 truncation does not bind

the full-length protein, it is likely that the SCA11 protein acts as a dominant negative by competing with the full-length protein for binding to another protein or proteins.

TTBK2 controls cilia length, trafficking and stability

To assess whether the more severe developmental defects in *Ttbk2*$^{sca11/gt}$ embryos were due to greater defects in cilia, we analyzed cilia in MEFs derived from embryos of each genotype of the *Ttbk2* allelic series. In *Ttbk2*$^{gt/+}$ cells, we found that a mean of 69.1 +/- 3.64 % of cells were ciliated (Figure 5A, I), whereas in *Ttbk2*$^{gt/gt}$ and *Ttbk2*$^{null/gt}$ an average of 45.9 +/- 3.66 % and 43.8 +/- 3.35 % of cells were ciliated, respectively (*Ttbk2*$^{gt/+}$ vs *Ttbk2*$^{gt/gt}$ p =0.0003; *Ttbk2*$^{gt/+}$ vs *Ttbk2*$^{null/gt}$ p<0.0001; *Ttbk2*$^{gt/gt}$ vs *Ttbk2*$^{null/gt}$ p= 0.9772; Figure 5B-C, I). There were clearly fewer cilia in *Ttbk2*$^{sca11/gt}$ cells, with an average of 18.9 +/- 3.65% of cells having a cilium (*Ttbk2*$^{null/gt}$ vs *Ttbk2*$^{sca11/gt}$ p<0.0001; Figure 5D, I). These findings suggest that the increased severity of the embryonic phenotypes correlates with a decrease in cilia number. While the mean cilia length was reduced in all of the *Ttbk2* mutants relative to *Ttbk2*$^{gt/+}$ cells, cilia length did not differ significantly between the different mutant allelic combinations (Figure 5J).

We also examined the percentage of cells with centrosomally localized TTBK2 in cells derived from embryos of each genotype, by calculating the percentage of cells with endogenous TTBK2 at the mother centriole or basal body in MEFs derived from each genotype. Relative to*Ttbk2*$^{gt/+}$, the percentage of cells with TTBK2 localized at the mother centriole/basal body in *Ttbk2*$^{gt/gt}$ trended towards being slightly reduced, though this was not statistically significant (Figure 5E-F, J; 38.1 +/- 9.11% for *Ttbk2*$^{gt/+}$ cells vs 25.5 +/- 2.76% for *Ttbk2*$^{gt/gt}$; p= 0.052). As expected, centriolar TTBK2 was further reduced in *Ttbk2*$^{null/gt}$ and *Ttbk2*$^{sca11/gt}$ cells (Figure 5G-H, J; 13.0 +/- 1.86% and 11.1 +/- 1.12%, respectively; *Ttbk2*$^{gt/+}$ vs *Ttbk2*$^{null/gt}$ p=0.001; *Ttbk2*$^{gt/+}$ vs *Ttbk2*$^{sca11/gt}$ p= 0.0006), but there was no significant difference between these two genotypes (Figure 5J; p= 0.9608), implying that the presence of TTBK2^{SCA11} does not interfere with full length TTBK2 function by impairing its localization to the presumptive basal body.

Our data indicate that hypomorphic *Ttbk2* mutants have shorter cilia in addition to forming cilia at a reduced frequency. We therefore hypothesize that TTBK2 may be required for ciliary trafficking and stability as well as for the initiation of ciliogenesis. To further investigate the role of TTBK2 in cilia structure and/or trafficking following initial assembly of the axoneme, we examined trafficking of HH pathway components in the cilia of MEFS of each genotype. The transmembrane protein SMO is critical for HH pathway activation, and becomes enriched within the cilium upon stimulation of the pathway with SHH or various agonists(11, 12). We found that the amount of SMO in the cilium upon stimulation of cells with SMO agonist (SAG) was comparable between $Ttbk2^{gt/+}$ cells and either $Ttbk2^{gt/gt}$ or $Ttbk2^{null/gt}$ cells, as measured by average intensity of SMO throughout the Acetylated α-Tubulin+ cilium (mean intensity of 82.2 +/- 3.43, 89.2 +/- 5.3, and 78.9 +/- 4.65 A.U, respectively). In contrast, SMO intensity was clearly reduced in the axonemes of $Ttbk2^{sca11/gt}$ cells (mean intensity of 51.0 +/- 3.78 A.U.) relative to $Ttbk2^{null/gt}$ ($p= 0.0003$), as well as each of the other genotypes (vs $Ttbk2^{gt/+}$ and $Ttbk2^{gt/gt}$ $p<0.0001$), consistent with the enhanced SHH signaling-related phenotypes observed in these mutant embryos (Figure 6A, B).

GLI2 is a transcription factor that mediates activation of target genes in response to HH ligands. GLI2 localizes to the tips of cilia, and becomes strongly enriched at the cilium tip in response to HH pathway activation(13) by SHH or SAG. There was no difference in GLI2 ciliary tip localization or intensity in response to SAG between $Ttbk2^{gt/+}$ and any of the mutant alleles (Figure S4A). KIF7 is the vertebrate homolog of the *Drosophila* protein COS2 and essential for the establishment and maintenance of the microtubule structure of the cilium in mammals, and for the stability of the axoneme(14, 15). Like GLI2, KIF7 normally becomes enriched at the tips of cilia in response to SAG, however in contrast to the results with GLI2, the percentage of cells with KIF7 localized to the tip of the cilium in the presence of SAG was significantly reduced in $Ttbk2^{sca11/gt}$ mutants relative to other genotypes ($Ttbk2^{gt/+}$: 82.2 +/-2.16%, $Ttbk2^{gt/gt}$: 75.6 +/- 1.73%, $Ttbk2^{null/gt}$: 62.6 +/- 7.93%, $Ttbk2^{sca11/gt}$: 37.8 +/- 1.1%; Figure 5C, D), and clearly less

than seen in *Ttbk2*$^{null/gt}$ (p= 0.012), suggesting that cilia structure or trafficking is impaired by the presence of the TTBK2^{SCA11} truncated protein.

Because KIF7 localization was disrupted in *Ttbk2*$^{sca11/gt}$ cells, we assessed other factors that control cilia trafficking and stability(15). Since the shorter cilia observed for each of the *Ttbk2* hypomorphic allele combinations relative to *Ttbk2*$^{gt/+}$ cells could be due to defects in IFT, we examined the localization of IFT components in MEFs of each genotype. Neither the IFT components IFT81, which localizes predominantly to the ciliary base and tip, nor IFT88, which is typically distributed throughout the axoneme, were appreciably altered in their localization (Figure S4B,D). Moreover, linescan analysis of IFT88 intensity plotted over the normalized axoneme length did not reveal any differences in distribution of IFT88 between these different genotypes (Figure S4C). This suggests that reduction of TTBK2 does not dramatically alter IFT and also argues that the exacerbated ciliary defects in *Ttbk2*$^{sca11/gt}$ cells are not the result of perturbed IFT trafficking.

Post-translational modifications of axonemal microtubules and axoneme stability are disrupted in *Kif7* mutants (12). We therefore examined tubulin polyglutamylation, a post-translational modification seen on ciliary microtubules that is important for establishing ciliary structure and length (16, 17). Intensity of polyglutamylated tubulin within the cilium was comparable between *Ttbk2*$^{gt/+}$ and *Ttbk2*$^{gt/gt}$ cells (mean intensity of 111.8 +/- 5.42 and 93.64 +/- 5.66 A.U. respectively) but was significantly reduced in *Ttbk2*$^{null/gt}$ cells (mean intensity of 75.8 +/- 4.85 A.U.) and further reduced in *Ttbk2*$^{sca11/gt}$ cells (mean intensity of 55.1 +/- 4.32 A.U.; Figure 6E, F). Reduction of tubulin polyglutamylation is associated with defects in cilium assembly and stability in a variety of organisms (16–18), although mechanisms that underlie these defects are incompletely understood. To examine cilium stability across the *Ttbk2* allelic series, we treated cells with nocodazole. Because the microtubule doublets of the ciliary axoneme are more stable than cytoplasmic microtubules, treatment of WT cells with nocodazole for a short period has a limited effect on cilia length or frequency(15). After treatment of MEFs

with nocodazole for 10 or 30 minutes, the percentage of ciliated cells in WT or *Ttbk2*$^{null/gt}$ cells decreased modestly (for WT, 77.7 +/- 1.73% of cells were ciliated at T0, 72.2 +/- 6.33% at 10 minutes, and 69.3 +/- 3.5% at 30 minutes; for *Ttbk2*$^{null/gt}$, 54.6 +/- 2.31% of cells were ciliated at T0, 45.5 +/- 0.64% at 10 minutes, and 46.3 +/- 1.96% at 30 minutes). In contrast, in *Ttbk2*$^{sca11/gt}$ cells treatment with nocodazole caused a rapid reduction in ciliated cells (from 26.6 +/- 3.38% at T0 to 13.6 +/- 0.62% after 10 minutes of treatment, and 8.1 +/- 1.24% after 30 minutes of treatment). The length of the remaining *Ttbk2*$^{sca11/gt}$ cilia reduced over time in a manner that was proportional to the other genotypes: for *Ttbk2*$^{sca11/gt}$ cells cilia length at 30 post nocodazole was 63.2% of the starting length, compared with 65.4% for *Ttbk2*$^{null/gt}$ and 55.9% for WT(Figure S4F). These data suggest that cilium stability is more compromised in *Ttbk2*$^{sca11/gt}$ cells than in *Ttbk2*$^{null/gt}$, consistent with the dominant negative nature of the *sca11* allele.

To further investigate the role of TTBK2 in cilium stability, we tested whether a pathway important in cilium suppression and disassembly was altered upon reduced TTBK2 function. KIF2A is an atypical kinesin of the Kinesin 13 family that mediates microtubule depolymerization in a number of cellular contexts (19). KIF2A was recently identified as a substrate of TTBK2 at the plus ends of cytoplasmic microtubules; in this context, phosphorylation by TTBK2 reduced KIF2A depolymerase activity, thereby stabilizing microtubules (20). Given this association, we tested whether the localization of KIF2A was altered in *Ttbk2* mutant cells. In WT MEFs, KIF2A was localized to the centrosome and was also occasionally seen within the ciliary axoneme (Figure 6H). Centrosome localization was maintained in the *Ttbk2* mutant alleles. However, quantification of KIF2A intensity at the base of ciliated cells showed that the level of KIF2A at the centrosome was increased in *Ttbk2*$^{null/gt}$ (mean pixel intensity of 43.1 +/- 1.96 A.U.) cells relative to *Ttbk*$^{gt/+}$ (mean pixel intensity of 19.98 +/- 0.92)or *Ttbk2*$^{gt/gt}$ (mean pixel intensity of 22.8 +/- 0.90 A.U). The intensity of KIF2A was further increased at the ciliary base of *Ttbk2*$^{sca11/gt}$ relative to all other genotypes (mean pixel intensity of 53.0 +/- 1.87 A.U., Figure 6I). This

suggests that KIF2A accumulates at the ciliary base when TTBK2 levels are reduced, contributing to the observed reduction in ciliated cells by promoting cilium disassembly.

Discussion

In this study, we show that the human SCA11- associated mutations to *Ttbk2* produce truncated proteins that interfere with the function of WT TTBK2 in cilia formation. Consistent with our previous data showing that familial SCA11-associated mutations are unable to restore primary cilia in null mutant cells, our analysis of *Ttbk2*$^{sca11/sca11}$ mutants revealed a phenotype that is essentially indistinguishable from that of our previously described ENU-induced null allele, *Ttbk2*$^{bby/bby}$. Like *Ttbk2*$^{bby/bby}$, homozygous SCA11 mutants lack cilia in all tissues examined at E10.5, and the cells of these mutants exhibit an identical set of cellular defects to those of embryos lacking *Ttbk2*. These results indicate that TTBK2^{SCA11} truncations are completely unable to function in mediating ciliogenesis, despite having an intact kinase domain and producing a protein product(8). This inability to function in ciliogenesis is likely the result of the SCA11-associated truncations lack of the C-terminus, which we and others have shown is required to target TTBK2 to the basal body and for its interaction with the distal appendage protein CEP164(4, 21, 22).

In our prior studies we also found that expression of TTBK2^{SCA11}-GFP in WT fibroblasts led to a modest but significant reduction in ciliogenesis(4), consistent with the classical definition of a dominant negative(23). We hypothesized based on this that the SCA11-associated mutations to *Ttbk2* function as antimorphic alleles. In the current work, we have present two major lines of evidence in support this hypothesis. First, we found that expression of WT TTBK2-GFP only partially rescues cilia formation in *Ttbk2*$^{sca11/sca11}$ mutant cells whereas full rescue is achieved by stable expression of the same construct in *Ttbk2*$^{null/null}$ cells. This is seen both at the level of ciliogenesis, where many fewer ciliated cells are found in rescued *Ttbk2*$^{sca11/sca11}$ and also with respect to the structure of the cilium: ARL13B localization is

significantly impaired in the rescued *Ttbk2*$^{sca11/sca11}$ relative to rescued null mutant cells. Second, we also show genetic evidence for the dominant negative function of *Ttbk2*^{sca11}. The combination of *Ttbk2*^{sca11} with a hypomorphic allele that produces a reduced amount of TTBK2 protein (*Ttbk2*^{gt}) results in more severe phenotypes than the null allele in combination with *Ttbk2*^{gt}.

We propose a model wherein TTBK2's functions in cilium assembly are highly dosage sensitive, with alterations in the amount of functional TTBK2 protein below a certain threshold causing a range of phenotypes related to defects in ciliary trafficking and signaling. In human SCA11 patients, the presence of SCA11 truncated protein is sufficient to cause a phenotype limited to a specific tissue- the cerebellum. In mice, we did not identify any changes in the architecture of the cerebellum between *Ttbk2*$^{sca11/+}$ animals and their WT siblings by 3 months of age. While we can't yet exclude the emergence of more subtle defects occurring at advanced age, it does not appear one allele of *Ttbk2*^{sca11} is sufficient to cause phenotypes recapitulating human SCA11 in the presence of a second WT allele of *Ttbk2*, (ie *Ttbk2*$^{sca11/+}$) in mice. However on a sensitized background with a reduced amount of full-length TTBK2, the dominant negative effects of TTBK2^{SCA11} become apparent, such as in the allelic series.

Our studies of the ciliary defects occurring in this allelic series of *Ttbk2* have also yielded valuable insights about the role of TTBK2 in cilia formation and trafficking. Our prior work based on a null allele of *Ttbk2* demonstrated the essential role played by this kinase in initiating cilium assembly upstream of IFT. However, examination of hypomorphic alleles in this study points to additional requirements for TTBK2 following initial cilium assembly. For example, cilia are shorter in cells derived from all of the hypomorphic *Ttbk2* alleles compared with WT or *Ttbk2*$^{gt/+}$ cells, pointing to a role for TTBK2 in cilia structure and trafficking. Identifying the molecular targets of TTBK2 in both cilium initiation and in ciliary trafficking and/or stability will be critically important to our understanding of the pathways that regulate ciliogenesis.

While we did not identify dramatic disruptions in the localization of IFT components in any of our *Ttbk2* hypomorphic alleles, we have uncovered a role for TTBK2 in the stability of the ciliary axoneme, with these defects becoming particularly evident in *Ttbk2*$^{sca11/gt}$ mutant cells. Consistent with a requirement for TTBK2 in cilia structure, KIF7 is reduced in *Ttbk2*$^{sca11/gt}$ cells compared with *Ttbk2*$^{null/gt}$ cells with respect to the percentage of cilia that are positive for KIF7, suggesting they have additional defects in the structure of the axoneme beyond those seen in the *Ttbk2*$^{null/gt}$ cells. The *Ttbk2*$^{sca11/gt}$ cells also exhibit a subset of the defects found in *Kif7*$^{-/-}$ cells, including a reduction in polyglutamylated tubulin(15). Unlike *Kif7*$^{-/-}$ cells however, we did not observe any reduction in tubulin acetylation in any of the *Ttbk2* hypomorphic cells. The *Ttbk2*$^{sca11/gt}$ cells do exhibit increased instability in the presence of nocodazole. The highly modified microtubules of the cilium are typically relatively resistant to this microtubule-depolymerizing drug(15, 24), and in WT or *Ttbk2*$^{null/gt}$ cells neither the proportion of ciliated cells nor the length of the cilium changes dramatically when the cells are treated with nocodazole for up to 30 minutes. In contrast, in the *Ttbk2*$^{sca11/gt}$ cells the percentage of ciliated cells drops dramatically upon treatment with nocodazole, consistent with a requirement for TTBK2 in the stability of the axonemal microtubules. In addition, increased levels of the microtubule depolymerizing kinesin KIF2A are present at the centrosome of ciliated cells in the *Ttbk2* hypomorphic mutants, with the highest amounts seen in *Ttbk2*$^{sca11/gt}$ cells. This suggests that TTBK2 may oppose the activity the PLK1-KIF2A cilium disassembly pathway, and that an increase in the activity of this pathway in the *Ttbk2* hypomorphic mutants contributes to the reduction in ciliated cells, in addition to defects in cilium stability.

The further reduction in TTBK2 function in the *Ttbk2*$^{sca11/gt}$ animals results in a greater perturbation of cilia than the defects seen in *Ttbk2*$^{null/gt}$ cells. These include reduced numbers of cilia, disrupted cilium stability, and impaired enrichment of signaling molecules such as SMO to the axoneme, although we have not yet precisely defined the biochemical mechanisms by which the human disease-associated truncations interfere with TTBK2 function. Our data argue

against a model where TTBK2^{SCA11} directly binds to full length TTBK2 and inhibits its function through a direct association. Rather, it seems more likely that TTBK2^{SCA11}, having lost critical regulatory motifs as well as the ability to efficiently translocate to the centrosome, may sequester some important TTBK2 substrate or substrates, resulting in the further impairment of cilia structure and signaling that in turn causes the modest exacerbations in Shh-dependent developmental patterning.

While our data indicate that the SCA11-associated *Ttbk2* mutations interfere with cilia formation and stability, pointing to a strong possibility that SCA11 pathology is related to disrupted ciliary signaling, we cannot exclude the possibility that TTBK2 has non-ciliary roles within the brain that could also contribute to neural degeneration. For example, TTBK2 phosphorylates Synaptic Vesicle Protein 2A, and this event is important for the formation and release of synaptic vesicles(25). The mechanisms of TTBK2 regulation as well as the specific substrates of this kinase in cilium assembly, as well as possible non-ciliary roles for TTBK2 within the brain are key topics in our ongoing research. Having shown that TTBK2^{SCA11} is both unable to mediate cilium assembly and also impairs the function of TTBK2^{WT} in ciliogenesis, another important area of investigation is the relationship between cilia and ciliary signaling pathways and the maintenance of neural connectivity and function.

Materials and Methods

Mouse Strains

The use and care of mice as described in this study was approved by the Institutional Animal Care and Use Committees of Memorial Sloan Kettering Cancer Center (approval number 02-06-013) and Duke University (approval number A246-14-10). All animal studies were performed in compliance with internationally accepted standards.

We made use of two previously described alleles of Ttbk2: *Ttbk2^{null}* is an ENU-induced allele (also called *Ttbk2^{bby}*)(4), and *Ttbk2^{sca11}* is a knockin recapitulating one of the familial

SCA11-associated mutations(8). Genotyping for both of these alleles was performed as previously described. *Ttbk2* "knockout first" genetrap (*Ttbk2*$^{tm1a(EUCOMM)Hmgu}$, here referred to *Ttbk2*^{gt}) targeted ES cells were purchased from the European Mutant Mouse Consortium. One clone (HEPD0767_5_E08, parental ESC line JM8A3.N1, agouti) was injected into host blastocysts by the Mouse Genetics Core Facility at Sloan Kettering Institute. Resulting chimeric male mice were bred to C57BL/6 females to test germline transmission and obtain heterozygous mice. PCR genotyping (F: ATACGGTTGAGATTCTTCTCCA, R1: TCTAGAGAATAGGAACTTCGG, R2: TGCAATTGCATGACCACGTAGT) yields a band corresponding to the mutant allele at 407bp and to the WT allele at 762bp.

Embryo and tissue dissection

To obtain embryos at the identified stages, timed matings were performed with the date of the vaginal plug considered embryonic day (E) 0.5. Pregnant dams were sacrificed by cervical dislocation and embryos were fixed in either 2% (E11.5 or earlier) or 4% (later than E11.5) paraformaldehyde (PFA) overnight at 4C. For cryosectioning, tissue was cryoprotected in 30% Sucrose overnight and embedded in Tissue Freezing Medium (General Data TFM-5). Tissue was sectioned at 16mm thickness.

To harvest tissues from adult mice, animals were anesthetized with 12.5mg/mL Avertin, and a transcardially perfused with of Phosphate Buffered Saline (PBS) followed by 4% PFA. Kidneys and brains were dissected and incubated in 4% PFA for an additional 2 hours at 4°C. Tissue was then prepared for cryosectioning as described above.

Cell culture and immunostaining

MEFs were isolated from embryos at either E10.5 or E12.5, and maintained as previously described(26). To induce cilia formation, cells were shifted from 10% to 0.5% fetal bovine serum (FBS) and maintained in low serum conditions for 48 hours. Cells were grown on

coverslips and fixed in 4% Paraformaldehyde (PFA) in Phosphate Buffered Saline (PBS) for 5 minutes at room temperature followed by methanol for 5 minutes at -20C. Cells were then washed in PBS + 0.2% Triton X-100 (PBT) and blocked in PBT + 5% FBS + 1% bovine serum albumin for 30 minutes. Cells were then incubated with primary antibodies diluted in blocking solution overnight at 4 □C, and finally incubated with Alexa-coupled secondary antibodies and DAPI in blocking solution for 30 minutes at room temperature and affixed to slides for microscopy. Embryonic and adult tissue sections were collected onto slides, dried, washed in PBT + 1% serum, and incubated with primary antibodies as described above.

Antibodies

The SMO antibody was raised in rabbits (Pocono Rabbit Farm and Laboratory Inc.) using antigens and procedures described(11); diluted 1:500. Antibodies against KIF7(14) (1:1000), ARL13B(27)(1:2000), GLI2(28)(1:2000) and TTBK2(8) have been previously described. Commercially available antibodies used in these studies were: mouse anti- NKX2.2, ISL1 (Developmental Studies Hybridoma Bank, each 1:10); mouse anti- Pericentrin, (BD Biosciences #611814, 1:500) γ-Tubulin (Sigma SAB4600239, 1:1000), Acetylated α-Tubulin (Sigma T6793, 1:1000), polyglutamylated Tubulin (Adipogen AG-20B-0020, 1:2000); rabbit anti-IFT88 (Proteintech 13967-1-AP, 1:500), TTBK2 (Proteintech 15072-1-AP, 1:1000), RAB8 (Proteintech 55296-1-AP, 1:500), Calbindin (Cell Signaling Technology 13176-S, 1:250), VGLUT2 (EMD Millipore AB2251, 1:2500).

Microscopy

Immuno-fluorescence images were obtained using a Zeiss AxioObserver wide field microscope equipped with an Axiocam 506mono camera and Apotome.2 optical sectioning with structured illumination. Z-stacks were taken at 0.24μm intervals. Whole mount images of embryos and tissues were captured with a Zeiss Discovery V12 SteREO microscope equipped

with an Axiocam ICc5 camera. Image processing and quantifications were performed using ImageJ. To quantify the signal intensities of ciliary proteins, Z stack images were captured using the 63X objective. A maximum intensity projection was then created for each image using ImageJ, background was subtracted. Cilia were identified by staining with Acetylated α-Tubulin and γ-Tubulin. Each cilium or portion of the cilium was highlighted using either the polygon tool or the line tool (for line-scan analysis), and the mean intensity was recorded for the desired channel (measured on an 8 bit scale), as described(15). Statistical analysis was done in Prism7 (GraphPad).

Western blotting and immunoprecipitation

HEK-293T cells were transfected with constructs for tagged proteins of interest using Lipofectamine 3000 (Thermo Fisher) according to the manufacturer's instructions. Constructs used were TTBK2^{FL}-GFP, TTBK2^{FL}-V5, TTBK2^{SCA11}-V5, TTBK2^{NTerm}-GFP (1-306aa), , Ttbk2^{Cterm}-GFP (306-1243aa).

For western blots, cells or tissues were lysed in buffer containing 10mM Tris/Cl pH7.5, 150mM NaCl, 0.5mM EDTA, 1% Triton, 1mM protease inhibitors (Sigma #11836170001) and 25mM β-glycerol phosphate (Sigma 50020), and total protein concentration was determined using a BSA Protein Assay Kit (Thermo Fisher #23227).

For co-IP experiments, cells were lysed in buffer containing 20mM Tris-HCl pH7.9, 150mM NaCl, 5mM EDTA, 1% NP-40, 5% glycerol, 1mM protease inhibitors and 25mM β-glycerol phosphate. Immunoprecipitation of lysates was performed using analysis was done using GFP-Trap beads (Chromotek GTA-20) blocked with 3% BSA in Co-IP lysis buffer overnight prior to pull-down. rabbit α-GFP (Invitrogen A11122, 1:10,000), mouse α-V5 (Invitrogen R96025, 1:7,000), HRP-conjugated secondaries (Jackson ImmunoResearch).

Cerebellum Quantification

Quantification of the cerebellar tissue was done using ImageJ software. Images for the molecular layer analysis were taken at 20x. For measuring the molecular layer, a line was drawn from the top of the PC cell soma to the pial surface and the distance was recorded. That same line was then brought down from the pial surface to the top of the nearest VGLUT2 puncta along that line, the distance was recorded, and a ratio was calculated. Measurements were pooled equally from both sides of the primary folia of the cerebellum, and from four slices per animal. Images for the VGLUT2 analysis were 10µm thick z-stacks taken at 63x. VGLUT2 puncta analysis was performed using the ImageJ "Analyze Particles" plug-in with the following stipulations: Size exclusion: 0.5-infinity, Circularity: 0-1. Measurements were pooled from 5 areas in the cerebellum, and from four slices per animal.

RT-PCR

RNA was extracted from brains dissected from p30 animals using the Qiagen RNeasy Mini Kit (Qiagen, 74104). cDNA was then made from 1µg of RNA using the BioRad iScript cDNA Synthesis Kit (BioRad, 1708891). PCR primers were designed to span the exon 4-5 boundary (F: ATGCTCACCAGGGAGAATGT, R: TGCATGACCACGTAGTTGAAA), lacZ (F: AGCAGCAGTTTTTCCAGTTC, R: CGTACTGTGAGCCAGAGTTG), and GAPDH (F: ACCACAGTCCATGCCATCAC, R: TCCACCACCCTGTTGCTGTA).

Acknowledgements

This work was supported by the National Institutes of Health [R00 HD076444 to SCG, R01 NS044385 to KVA], and the National Ataxia Foundation [Young Investigator in SCA Award to SCG]. We are grateful to Jonathan Eggenschwiler and Dario Alessi for reagents.

References

1. Goetz,S.C. and Anderson,K.V. (2010) The primary cilium: a signalling centre during vertebrate development. *Nat. Rev. Genet.*, **11**, 331–344.

2. Métin,C. and Pedraza,M. (2014) Cilia: traffic directors along the road of cortical development. *Neuroscientist*, **20**, 468–482.

3. Ruat,M., Roudaut,H., Ferent,J. and Traiffort,E. (2011) Hedgehog trafficking, cilia and brain functions. *Differentiation*.

4. Goetz,S.C., Liem,K.F.,Jr and Anderson,K.V. (2012) The spinocerebellar ataxia-associated gene Tau tubulin kinase 2 controls the initiation of ciliogenesis. *Cell*, **151**, 847–858.

5. Houlden,H., Johnson,J., Gardner-Thorpe,C., Lashley,T., Hernandez,D., Worth,P., Singleton,A.B., Hilton,D.A., Holton,J., Revesz,T., *et al.* (2007) Mutations in TTBK2, encoding a kinase implicated in tau phosphorylation, segregate with spinocerebellar ataxia type 11. *Nat. Genet.*, **39**, 1434–1436.

6. Bauer,P., Stevanin,G., Beetz,C., Synofzik,M., Schmitz-Hübsch,T., Wüllner,U., Berthier,E., Ollagnon-Roman,E., Riess,O., Forlani,S., *et al.* (2010) Spinocerebellar ataxia type 11 (SCA11) is an uncommon cause of dominant ataxia among French and German kindreds. *J. Neurol. Neurosurg. Psychiatry*, **81**, 1229–1232.

7. Lindquist,S.G., Møller,L.B., Dali,C.I., Marner,L., Kamsteeg,E.-J., Nielsen,J.E. and Hjermind,L.E. (2017) A Novel TTBK2 De Novo Mutation in a Danish Family with Early-Onset Spinocerebellar Ataxia. *Cerebellum*, **16**, 268–271.

8. Bouskila,M., Esoof,N., Gay,L., Fang,E.H., Deak,M., Begley,M.J., Cantley,L.C., Prescott,A., Storey,K.G. and Alessi,D.R. (2011) TTBK2 kinase substrate specificity and the impact of spinocerebellar-ataxia-causing mutations on expression, activity, localization and development. *Biochem. J.*, **437**, 157–167.

9. Jiang,K., Toedt,G., Montenegro Gouveia,S., Davey,N.E., Hua,S., van der Vaart,B., Grigoriev,I., Larsen,J., Pedersen,L.B., Bezstarosti,K., *et al.* (2012) A Proteome-wide screen for mammalian SxIP motif-containing microtubule plus-end tracking proteins. *Curr. Biol.*, **22**, 1800–1807.

10. Knippschild,U., Krüger,M., Richter,J., Xu,P., García-Reyes,B., Peifer,C., Halekotte,J., Bakulev,V. and Bischof,J. (2014) The CK1 Family: Contribution to Cellular Stress Response and Its Role in Carcinogenesis. *Front. Oncol.*, **4**, 96.

11. Rohatgi,R., Milenkovic,L. and Scott,M.P. (2007) Patched1 Regulates Hedgehog Signaling at the Primary Cilium. *Science*, **317**, 372–376.

12. Rohatgi,R., Milenkovic,L., Corcoran,R. and Scott,M. (2009) Hedgehog signal transduction by Smoothened: Pharmacologic evidence for a 2-step activation process. *Proc. Natl. Acad. Sci. U. S. A.*

13. Haycraft,C.J., Banizs,B., Aydin-Son,Y., Zhang,Q., Michaud,E.J. and Yoder,B.K. (2005) Gli2 and Gli3 localize to cilia and require the intraflagellar transport protein polaris for processing and function. *PLoS Genet.*, **1**, e53.

14. Liem,K.F., He,M., Ocbina,P.J.R. and Anderson,K.V. (2009) Mouse Kif7/Costal2 is a cilia-

associated protein that regulates Sonic hedgehog signaling. *Proc. Natl. Acad. Sci. U. S. A.*, **106**, 13377–13382.

15. He,M., Subramanian,R., Bangs,F., Omelchenko,T., Liem,K.F., Kapoor,T.M. and Anderson,K.V. (2014) The kinesin-4 protein Kif7 regulates mammalian Hedgehog signalling by organizing the cilium tip compartment. *Nat. Cell Biol.*, **16**, 663–672.

16. Pathak,N., Obara,T., Mangos,S., Liu,Y. and Drummond,I.A. (2007) The zebrafish fleer gene encodes an essential regulator of cilia tubulin polyglutamylation. *Mol. Biol. Cell*, **18**, 4353–4364.

17. Pathak,N., Austin,C.A. and Drummond,I.A. (2011) Tubulin tyrosine ligase-like genes ttll3 and ttll6 maintain zebrafish cilia structure and motility. *J. Biol. Chem.*, **286**, 11685–11695.

18. Lin,H., Zhang,Z., Guo,S., Chen,F., Kessler,J.M., Wang,Y.M. and Dutcher,S.K. (2015) A NIMA-Related Kinase Suppresses the Flagellar Instability Associated with the Loss of Multiple Axonemal Structures. *PLoS Genet.*, **11**, e1005508.

19. Walczak,C.E., Gayek,S. and Ohi,R. (2013) Microtubule-depolymerizing kinesins. *Annu. Rev. Cell Dev. Biol.*, **29**, 417–441.

20. Watanabe,T., Kakeno,M., Matsui,T., Sugiyama,I., Arimura,N., Matsuzawa,K., Shirahige,A., Ishidate,F., Nishioka,T., Taya,S., *et al.* (2015) TTBK2 with EB1/3 regulates microtubule dynamics in migrating cells through KIF2A phosphorylation. *J. Cell Biol.*, **210**, 737–751.

21. Čajánek,L. and Nigg,E.A. (2014) Cep164 triggers ciliogenesis by recruiting Tau tubulin kinase 2 to the mother centriole. *Proc. Natl. Acad. Sci. U. S. A.*, **111**, E2841–50.

22. Oda,T., Chiba,S., Nagai,T. and Mizuno,K. (2014) Binding to Cep164, but not EB1, is essential for centriolar localization of TTBK2 and its function in ciliogenesis. *Genes Cells*.

23. Herskowitz,I. (1987) Functional inactivation of genes by dominant negative mutations. *Nature*, **329**, 219–222.

24. Sharma,N., Kosan,Z.A., Stallworth,J.E., Berbari,N.F. and Yoder,B.K. (2011) Soluble levels of cytosolic tubulin regulate ciliary length control. *Mol. Biol. Cell*, **22**, 806–816.

25. Zhang,N., Gordon,S.L., Fritsch,M.J., Esoof,N., Campbell,D.G., Gourlay,R., Velupillai,S., Macartney,T., Peggie,M., van Aalten,D.M.F., *et al.* (2015) Phosphorylation of synaptic vesicle protein 2A at Thr84 by casein kinase 1 family kinases controls the specific retrieval of synaptotagmin-1. *J. Neurosci.*, **35**, 2492–2507.

26. Ocbina,P.J.R. and Anderson,K.V. (2008) Intraflagellar transport, cilia, and mammalian Hedgehog signaling: analysis in mouse embryonic fibroblasts. *Dev. Dyn.*, **237**, 2030–2038.

27. Larkins,C.E., Aviles,G.D.G., East,M.P., Kahn,R.A. and Caspary,T. (2011) Arl13b regulates ciliogenesis and the dynamic localization of Shh signaling proteins. *Mol. Biol. Cell*, **22**, 4694–4703.

28. Cho,A., Ko,H.W. and Eggenschwiler,J.T. (2008) FKBP8 cell-autonomously controls neural tube patterning through a Gli2- and Kif3a-dependent mechanism. *Dev. Biol.*, **321**, 27–39.

Legends to Figures

Figure 1. The phenotype of *Ttbk2*$^{sca11/sca11}$ embryos is identical to that of the null allele.

(A) Representative wild-type, *Ttbk2*$^{null/null}$, and *Ttbk2*$^{sca11/sca11}$ E10.5 embryos. Scale bar = 1mm.

(B-C, E-F) Transverse sections through neural tubes of wild-type (B-C) and *Ttbk2*$^{sca11/sca11}$ (E-F) E10.5 embryos. Sections were taken at the level of the forelimbs and immunostained for ISL1 (B, E) to label differentiated motor neurons or NKX2.2 and OLIG2 (C, F) to label V3 interneuron progenitors and motor neuron progenitors, respectively. Scale bar = 100µm.

(D, G) Mesenchymal cells surrounding neural tube of E10.5 WT and *Ttbk2*$^{sca11/sca11}$ embryos, immunostained for ARL13B to label cilia (green) and γ-Tubulin (red). Scale bar = 20µm.

Figure 2. A SCA11-associated allele of *Ttbk2* interferes wild-type TTBK2 function in cilia formation.

(A, B) A comparison of rescue of cilia formation by WT TTBK2-GFP in MEFs derived from *Ttbk2*$^{null/null}$ embryos vs *Ttbk2*$^{sca11/sca11}$ embryos. A representative field of cells from each condition is shown in (A) immunostained for ARL13B (green) and γ-Tubulin (red). Scale bar = 20µm. The mean percent of ciliated cells in *Ttbk2*$^{null/null}$ MEFs versus *Ttbk2*$^{sca11/sca11}$ MEFs after rescue with TTBK2^{WT} is shown in (B). The graph represents the average of 6 fields of cells across two independent experiments (n= . Error bars represent SEM. p=0.0002.

(C-E) A comparison of cilia morphology in WT cells, *Ttbk2*$^{null/null}$ MEFs rescued with TTBK2-GFP, and *Ttbk2*$^{sca11/sca11}$ MEFs rescued with TTBK2-GFP. (C) Depicts two representative images of cilia of each condition immunostained for ARL13B (green) and γ-Tubulin (red). Scale bar = 2µm. ARL13B fluorescence intensity is shown in (D). ARL13b intensity is lower in *Ttbk2*$^{sca11/sca11}$+TTBK2-GFP compared to both WT and *Ttbk2*$^{null/null}$ +TTBK2-GFP ($p<0.0001$), however the mean cilia length is not different between these conditions (E).

Figure 3. A *Ttbk2* allelic series highlights reveals enhanced Shh-related phenotypes in *Ttbk2*$^{sca11/gt}$ embryos.

(A-D) Representative E15.5 embryos of each of the indicated Ttbk2 allelic combinations. Scale bar = 3mm. * Denotes duplicated digits. Insets are 1.5X enlargements of the hindlimbs shown in each image.

(E-H) Transverse sections through the neural tube of E10.5 embryos of the indicated genotypes. Sections were taken at the forelimb level and immunostained for the motor neuron marker ISL1. Scale bar = 100µm.

(I-L) Representative transverse sections through E10.5 neural tubes of embryos of each indicated genotype immunostained for NKX2.2 (green) to label V3 interneuron progenitors and OLIG2 (red) to label motor neuron progenitors.

Figure 4. TTBK2 homodimerizes through its C-terminus.

(A) A schematic representing the various TTBK2 truncations used for co-immunoprecipitation. TTBK2^{FL} is comprised of full length mouse TTBK2. TTBK2^{NTerm} is comprised of amino acids 1-306, including the kinase domain. TTBK2^{CTerm} is composed of TTBK2 amino acids following the kinase domain: 306-1243. TTBK2^{SCA11} corresponds to one of the disease-associated mutations, and includes amino acids 1-443. Each is tagged with either V5 or GFP at the N-terminus as indicated in B and C.

(B) Construct were expressed together as indicated in HEK 293T cells, which were lysed and subjected to immunoprecipitation using anti-GFP conjugated beads. Full length TTBK2 tagged with V5 (TTBK2^{FL}-V5) was co-precipitated with full length TTBK2 tagged with GFP (TTBK2^{FL}-GFP, , with was performed on HEK-293T cells that were transfected with either V5 or GFP-tagged full-length TTBK2 (TTBK2^{FL}) or various GFP-tagged truncations of TTBK2 (TTBK2^{Cterm} and TTBK2^{Nterm}). Co-IPs were performed with GFP-conjugated beads (Chromotek). TTBK2^{FL} interacts with TTBK2^{FL} and TTBK2^{Cterm}, but not TTBK2^{Nterm}. (B) Co-Immunoprecipitation

demonstrating that TTBK2^{FL} does not interact with the TTBK2^{sca11} truncation, and TTBK2^{sca11} does not interact with TTBK2^{sca11}.

Figure 5. Ciliary defects are evident in *Ttbk2* hypomorphic mutant cells.

(A-D) Representative images of MEFs taken from the embryos of the indicated and serum starved for 48-hours to induce ciliogenesis. Cilia are immunostained for ARL13b (green) to label cilia and γ-Tubulin (red) to label centrosomes. Scale bar = 20μm.

(E-H) Localization of endogenous TTBK2 (green) in MEFs of each indicated genotype. Cells were counterstained with γ-Tubulin (red) to label centrosomes and Acetylated α-Tubulin (magenta) to label cilia. Lower panels show zoomed images of from individual cells seen in the top panel. Scale bar = 10μm, 2μm for zoomed panels.

(I) Quantification of the percentage of ciliated cells from MEFs of each genotype following 48 hours of serum starvation. Cilia frequency is reduced in all mutants compared with heterozygous cells, and is further reduced in *Ttbk2*$^{sca11/gt}$ cells relative to *Ttbk2*$^{null/gt}$. Bars represent the mean percentage of ciliated cells across 3 experiments with 3 replicates each (n= 289, *Ttbk2*$^{gt/+}$; n= 252, *Ttbk2*$^{gt/gt}$; n= 584, *Ttbk2*$^{null/gt}$; n= 340 *Ttbk2*$^{sca11/gt}$). Error bars denote SEM.

(J) Quantification of cilia length in MEFS of each genotype following 48 hours of serum starvation. Cilia in each of the mutant MEFs were significantly shorter than heterozygous cells, but did not differ significantly from each other.

(K) Quantification of the percentage of cells with endogenous TTBK2 localized to the centrosome following 48 hours of serum withdrawal. Ttbk2 mutant cells, particularly Ttbk2$^{null/gt}$ and Ttbk2$^{sca11/gt}$ have reduced TTBK2 at the centrosome, however these two genotypes did not differ from one another with respect to TTBK2 localization.

For I-K, stars denote statistical comparisons between the indicated groups (2 way ANOVA with Tukey-Kramer post hoc test, **** denotes $p< 0.0001$, *** denotes $p<0.001$, ** denotes $p<0.01$, * denotes $p<0.05$.)

Figure 6. Localization of key ciliary proteins is impaired in *Ttbk2*$^{sca11/gt}$ cilia.

(A, B) SMO localization in heterozygous and *Ttbk2* mutant MEFs. Immunofluorescence for SMO (magenta) is shown for each of the indicated genotypes in (A), with centrosomes stained for γ-Tubulin (red), and the ciliary axoneme labeled with Acetylated α-Tubulin (green). Cells were serum starved for 24 hours before being treated with DMSO (-SAG) or 200nm SAG (+SAG) for an additional 24 hours. Two representative images are shown for each condition. (B) depicts a quantification of pixel intensity of SMO within the ciliary axoneme of each genotype upon stimulation with SAG. Bars represent the mean intensity of 50 measurements across 3 replicates for each genotype. Error bars depict SEM. Statistical comparison was performed by 2-way ANOVA with Tukey-Kramer post-hoc test. *Ttbk2*$^{sca11/gt}$ cells display reduced SMO intensity within the cilium compared with each of the other genotypes ($p<0.0001$ vs *Ttbk2*$^{gt/+}$ and *Ttbk2*$^{gt/gt}$; $p= 0.0003$ vs *Ttbk2*$^{null/gt}$).

(C, D) Localization of KIF7 (magenta) to the ciliary tip in MEFs of each indicated genotype. In (C) cells are counterstained for γ-Tubulin (red) to label centrosomes and Acetylated α-Tubulin (green) to label the axonemes. Three representative images are shown for each genotype. The percentage of cilia with KIF7 correctly localized to the ciliary tip upon treatment with SAG is shown in (D). We find that the frequency of KIF7 localization is reduced in *Ttbk2*$^{sca11/gt}$ cells compared with other genotypes ($p= 0.0003$ vs *Ttbk2*$^{gt/+}$; $p=0.0009$ vs *Ttbk2*$^{gt/gt}$; $p=0.012$ vs *Ttbk2*$^{null/gt}$.)

(E, F) Polyglutamylated tubulin localization in cilia of MEFs derived from embryos of the indicated genotypes. Immunostaining for GT335, which recognizes polyglutamylated tubulin (magenta) as well as PCNT (red) to label centrosomes and Acetylated α-Tubulin (green) to label cilia is shown in (E). A quantification of the pixel intensity of GT335 within cilia is shown in (F). Polyglutamylated tubulin levels are reduced in *Ttbk2*$^{sca11/gt}$ relative to the other genotypes of the allelic series ($p<0.0001$ vs vs *Ttbk2*$^{gt/+}$; $p<0.0001$ vs vs *Ttbk2*$^{gt/gt}$; $p= 0.0327$ vs *Ttbk2*$^{null/gt}$).

(G) Wild type, *Ttbk2*$^{bby/gt}$, and *Ttbk2*$^{sca11/gt}$ MEFs were treated with 10µM Nocodazole for 10-30 minutes and percentage of ciliated cells was determined. While in WT and *Ttbk2*$^{null/gt}$ cells the percentage of ciliated cells reduced only slightly within 30 minutes, cilia were rapidly lost in *Ttbk2*$^{sca11/gt}$ MEFs upon treatment with nocodazole (p= 0.0112).

(H, I) Immunostaining for KIF2A (magenta) in MEFs derived from embryos of the indicated genotypes of the Ttbk2 allelic series shown in (H). MEFs were serum starved for 48 hours. Centrosomes are labeled with γ-Tubulin (red) and cilia are stained for Acetylated α-Tubulin (green). Pixel intensity of KIF2A at the centrosome is quantified in (I). While we detected no significant difference between *Ttbk2*$^{gt/+}$ and *Ttbk2*$^{gt/gt}$, *Ttbk2*$^{null/gt}$ and *Ttbk2*$^{sca11/gt}$ cells have increased levels of KIF2A at the centrosome, and KIF2A is further increased in *Ttbk2*$^{sca11/gt}$. (p<0.0001 for all).

n=50 cilia pooled from 3 biological replicates.

Scale bar = 5µm

Figure S1. Cellular defects in *Ttbk2*$^{sca11/sca11}$ cells recapitulate those seen in *Ttbk2*$^{null/null}$.

(A,B) MEFs of the indicated genotype were serum starved for 48 hours and immunostained for IFT88 (green) as well as γ-Tubulin (red) to label centrosomes and Acetylated α-Tubulin (magenta) to label the axonemes of cilia. *Ttbk2*$^{sca11/sca11}$ cells lack cilia and also lack IFT88 at the mother centriole.

(C,D). Serum starved MEFs were treated as above and stained for CP110 (green) and γ-Tubulin (red). *Ttbk2*$^{sca11/sca11}$ cells retain CP110 on both centrosomes in the absence of serum.

Scale bar = 5µm.

Figure S2. *Ttbk2*$^{sca11/+}$ mice do not show signs of cerebellar degeneration.

(A,B) Representative sagittal sections through the cerebellum of mice of the indicated genotype. Purkinje cells are labeled with Calbindin (red) and excitatory synapses from the climbing fibers onto the Purkinje cell dendrites are labeled with VGLUT2 (green). Scale bar = 50µm.

(C,D) Measurements for the molecular layer length and VGLUT2 extension were made from four separate primary folia, pooled from three individual mice for each condition. Error bars denote SEM. The molecular layer length and VGLUT2 extension are unchanged between wild-type and *Ttbk2*$^{sca11/+}$.

Figure S3. *Ttbk2*^{gt} is a hypomorphic allele of *Ttbk2*.

(A) Schematic of the *Ttbk2* gene trap (*Ttbk2*^{gt}) targeting design (schematic adapted from IMPC).

(B) RT-PCR analysis of WT splicing in *Ttbk2*$^{gt/gt}$. RNA from 3 biological replicate brains per genotype was used, and primers targeting the exon 4-5 boundary show that WT transcript is still being made in *Ttbk2*$^{gt/gt}$ mice.

(C) P30 mice showing phenotypic differences between *Ttbk2*$^{gt/+}$ and *Ttbk2*$^{gt/gt}$.

(D) H&E staining of neural cortex and kidney tissue from 6mo old *Ttbk2*$^{gt/gt}$ mice showing hydrocephaly and polycyctic kidneys. Scale bar = 1mm.

(E) Western blot showing decreased TTBK2 protein expression (150kDa) between *Ttbk2*^{WT}, *Ttbk2*$^{gt/+}$, and *Ttbk2*$^{gt/gt}$. No TTBK2 protein is seen in *Ttbk2*$^{bby/bby}$. Bands seen at 100kDa are non-specific, γ-Tubulin or acetylated α-Tubulin is the loading control.

Figure S4 Trafficking defects in the *Ttbk2* allelic series cilia.

(A,D) Immunostaining in MEFs of each indicated genotype of Gli2 (magenta), γ-Tubulin (red) to label centrosomes and Acetylated α-Tubulin (green) to label the axonemes (A). Quantification of Gli2 pixel intensity at the tip of the axoneme is not significant between genotypes (D). Scale bar = 5µm

(B, E) Immunostaining of IFT88 (magenta) shows no major localization defects between indicated genotypes (B). Average IFT88 pixel intensity along pooled axonemes is not significant (data not shown). Line profiles that show IFT88 pixel intensity from the base of the ciliary axoneme to the tip shows that *Ttbk2*$^{null/gt}$ has a higher accumulation at the tip than other genotypes (E).

(C,F) Immunostaining of IFT81 (magenta) showing representative localization between indicated genotypes (C). Average IFT81 pixel intensity along pooled axonemes is not significant (data not shown). Line profiles that show IFT81 pixel intensity from the base of the ciliary axoneme to the tip shows that *Ttbk2*$^{gt/gt}$, *Ttbk2*$^{null/gt}$, and *Ttbk2*$^{sca11/gt}$ have an accumulation of IFT81 pixel intensity at the base relative to the tip compared to *Ttbk2*$^{gt/+}$ (F).

(G) Wild type, *Ttbk2*$^{bby/gt}$, and *Ttbk2*$^{sca11/gt}$ MEFs were treated with 10μM Nocodazole for 10-30 minutes and cilia length was measured. No significant changes were seen in ciliary length between genotypes over time.

n=50 cilia pooled from 3 biological replicates.

Cross	Stage	Total Number	Number of mutants	Percent Mutant
GT X GT	E14.5	81	17	20.9
	E17.5-P0	183	44	24.0
GT X Null	E14.5	67	21	31.3
	E17.5-P0	43	8	18.6
GT X SCA11	E14.5	99	22	22.2
	E17.5-P0	63	6	9.5

Table S1. Numbers of mutants obtained from allelic series crosses.

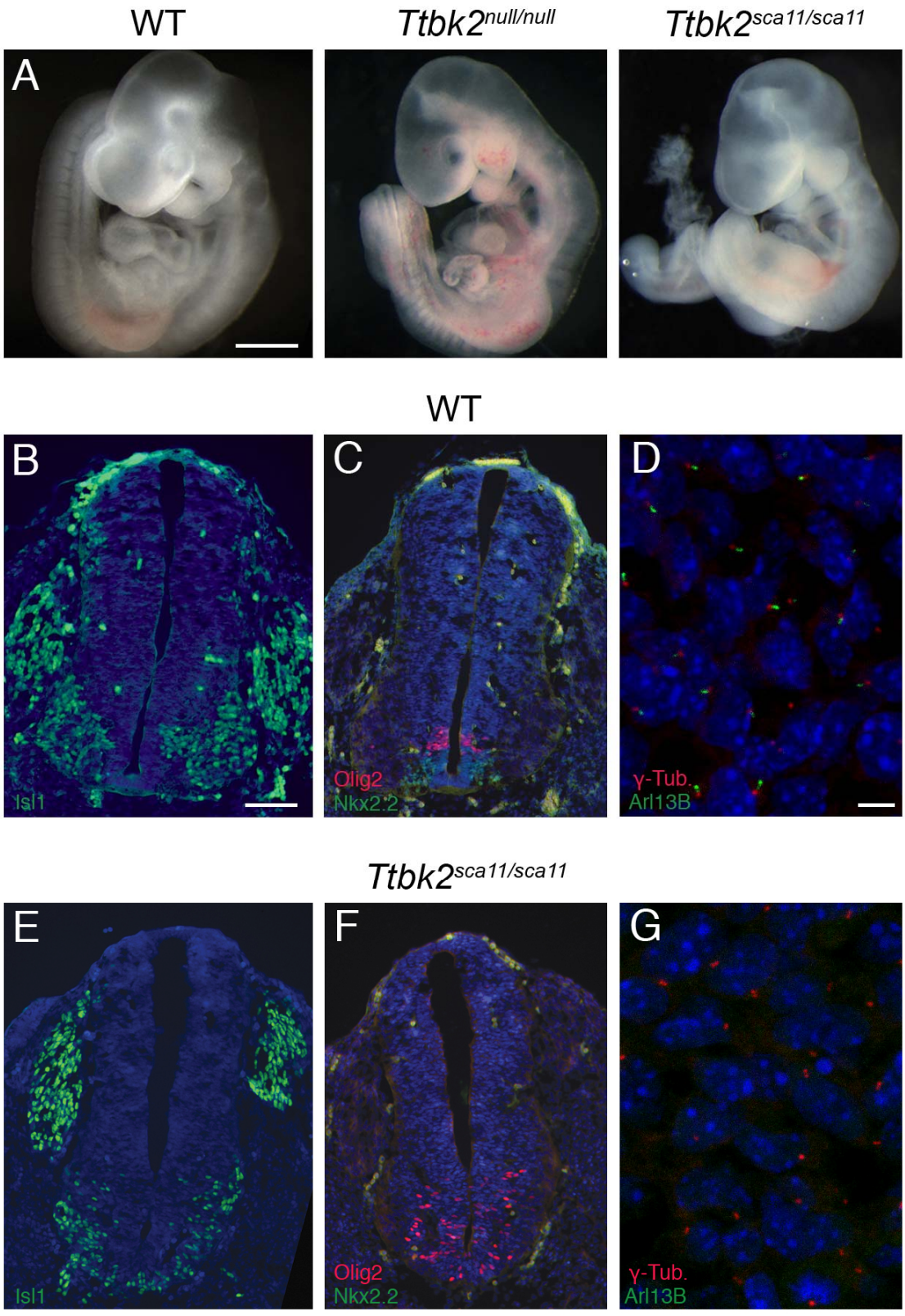

Figure 1

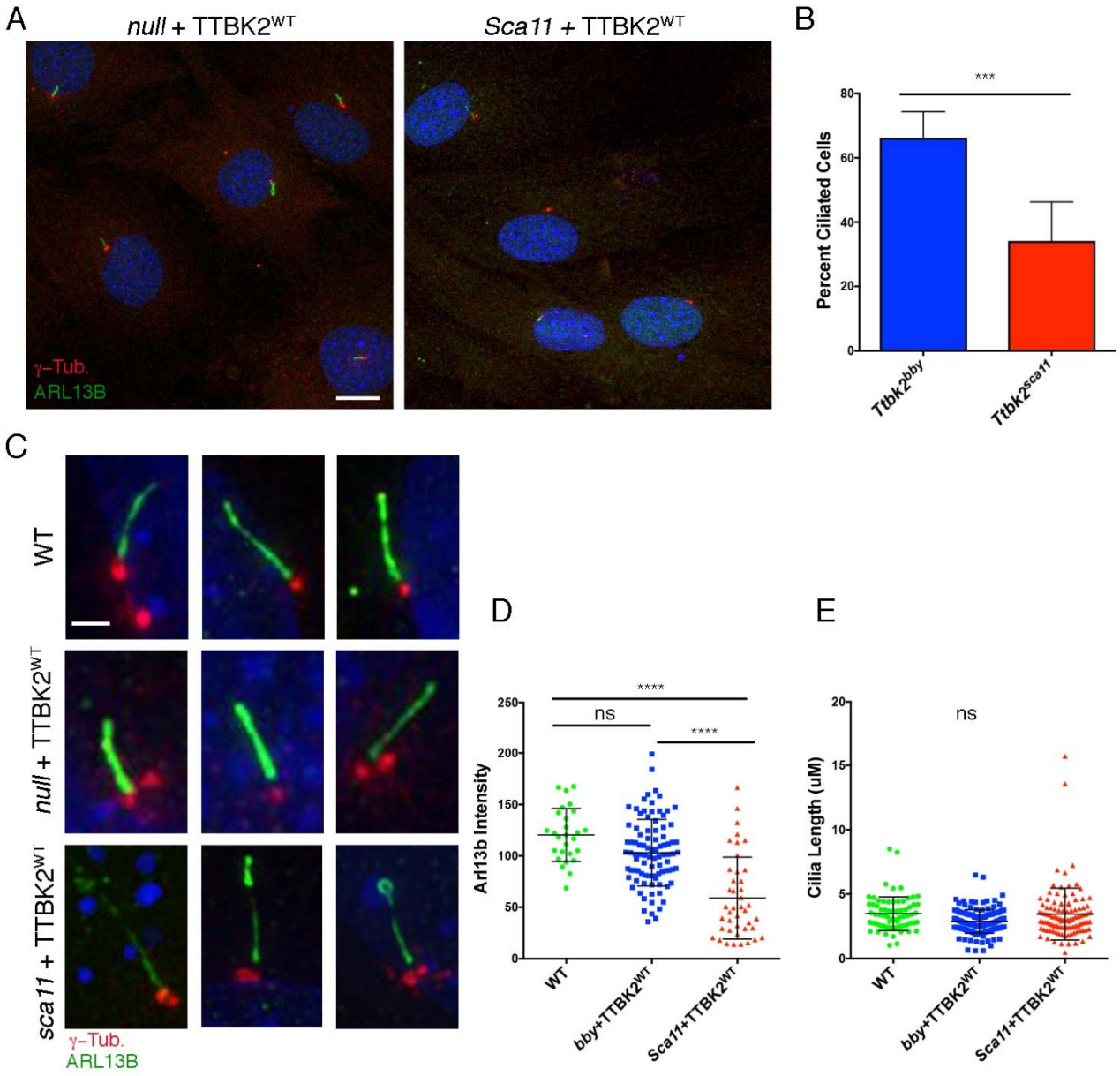

Figure 2

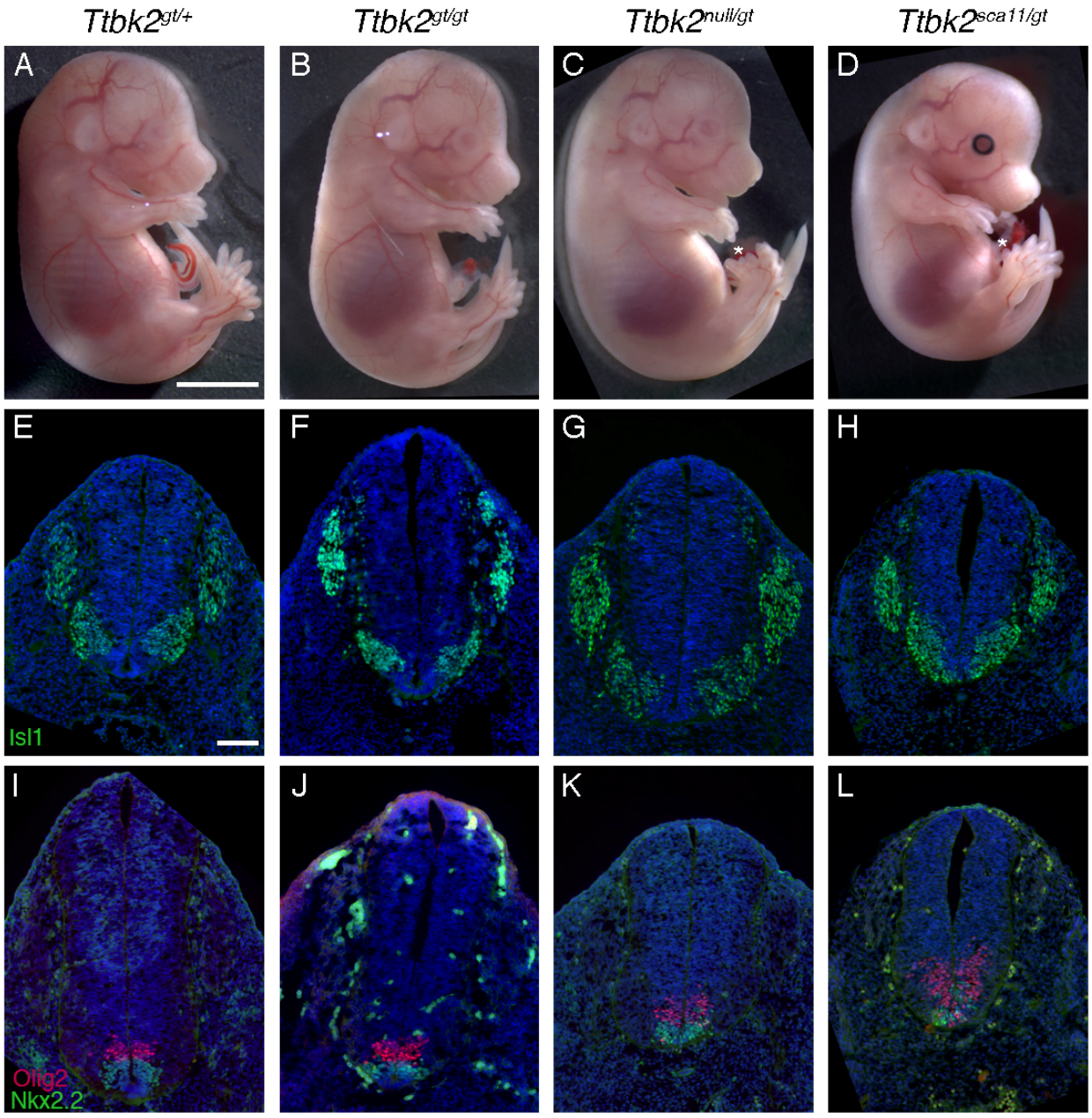

Figure 3

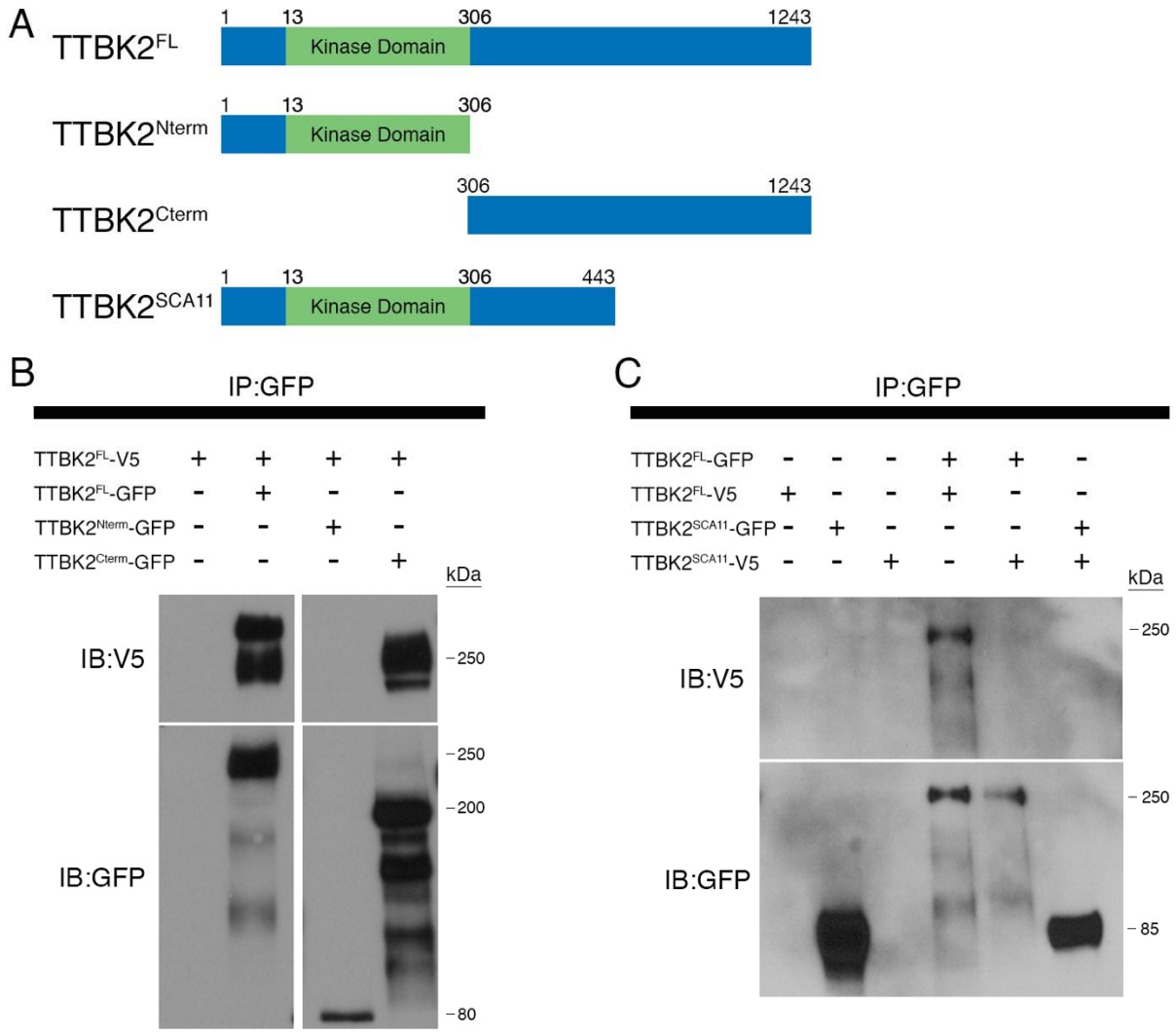

Figure 4

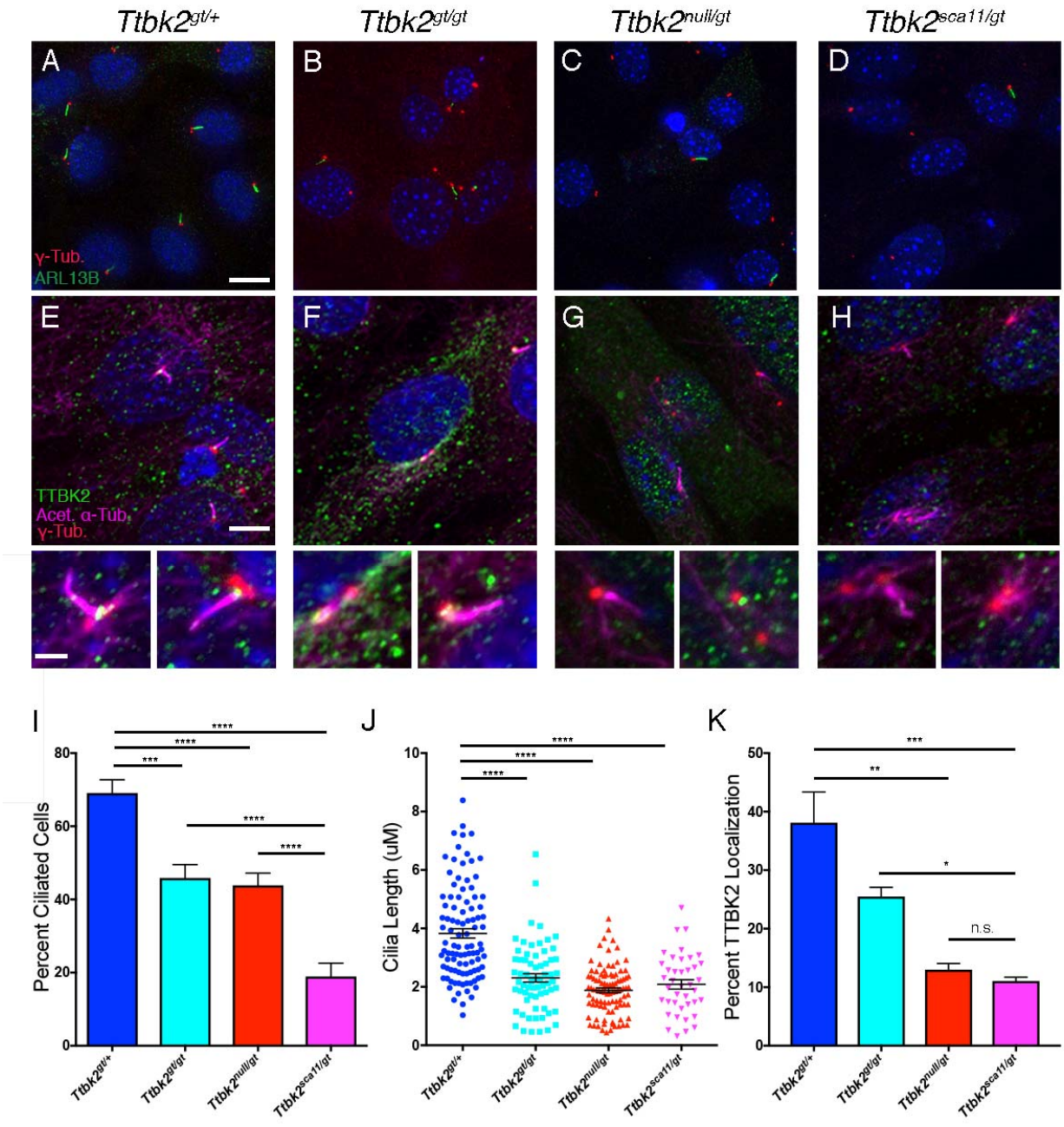

Figure 5

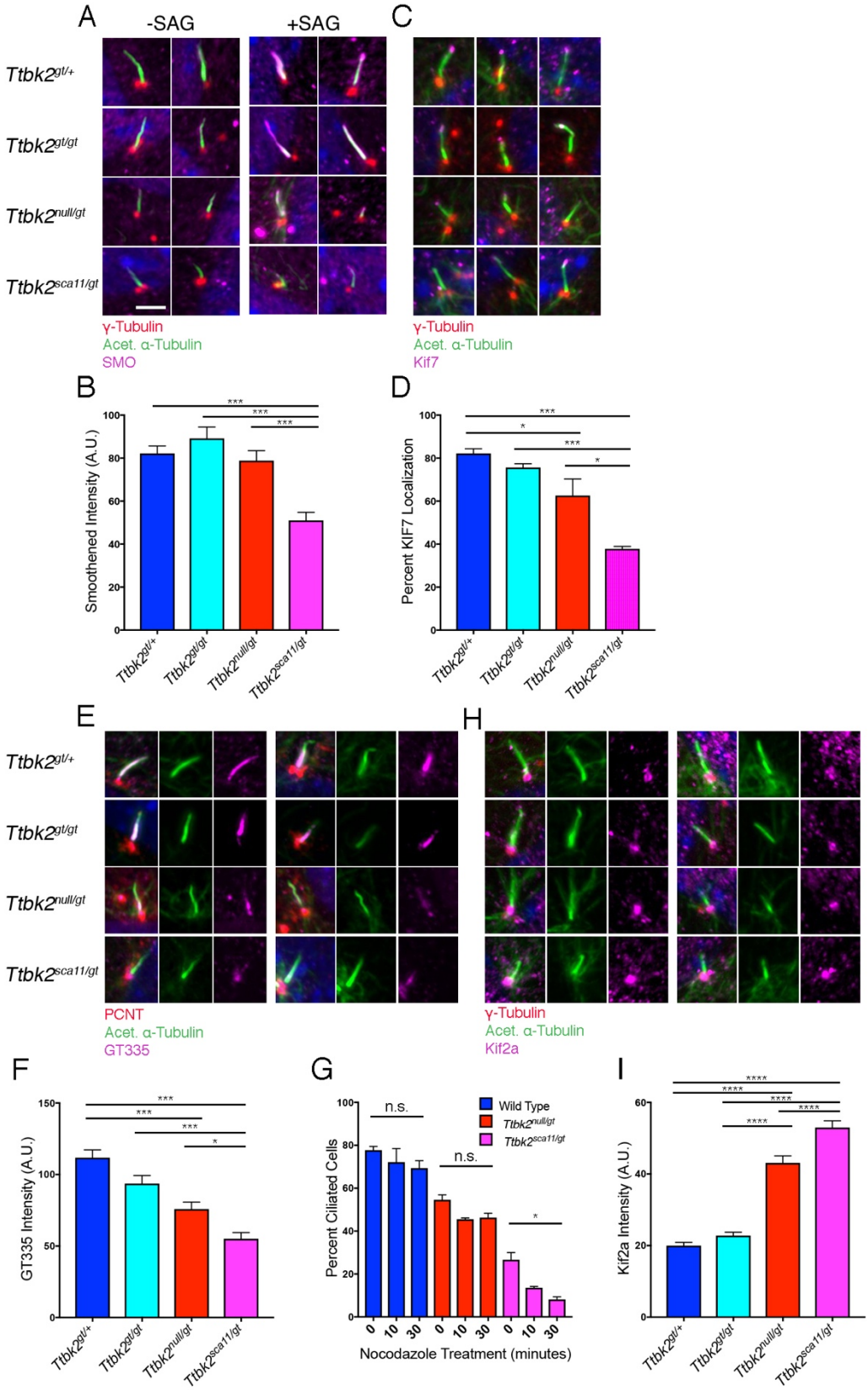

Figure 6

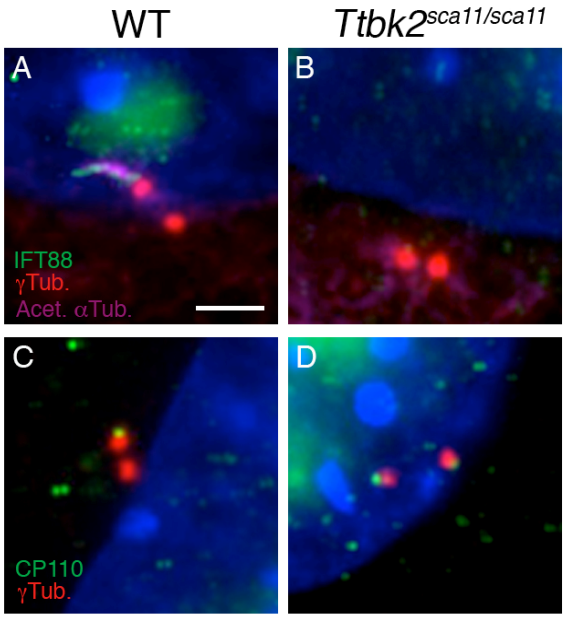

Figure S1

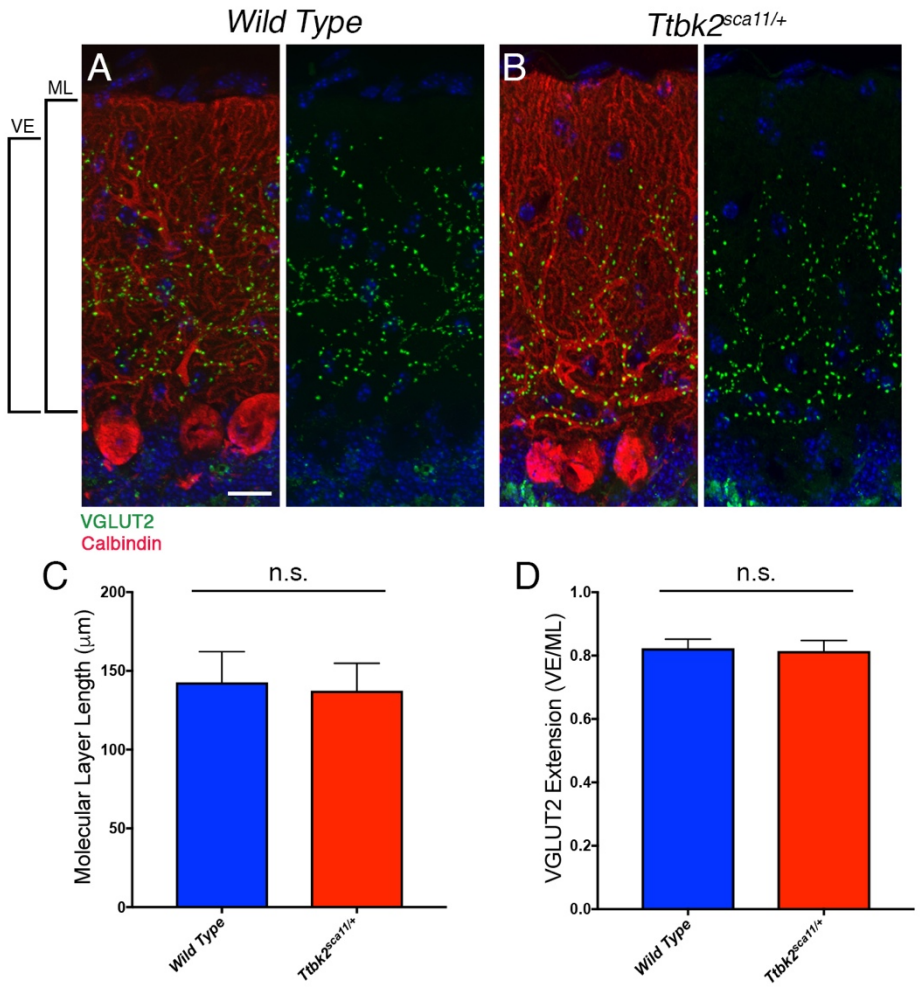

Figure S2

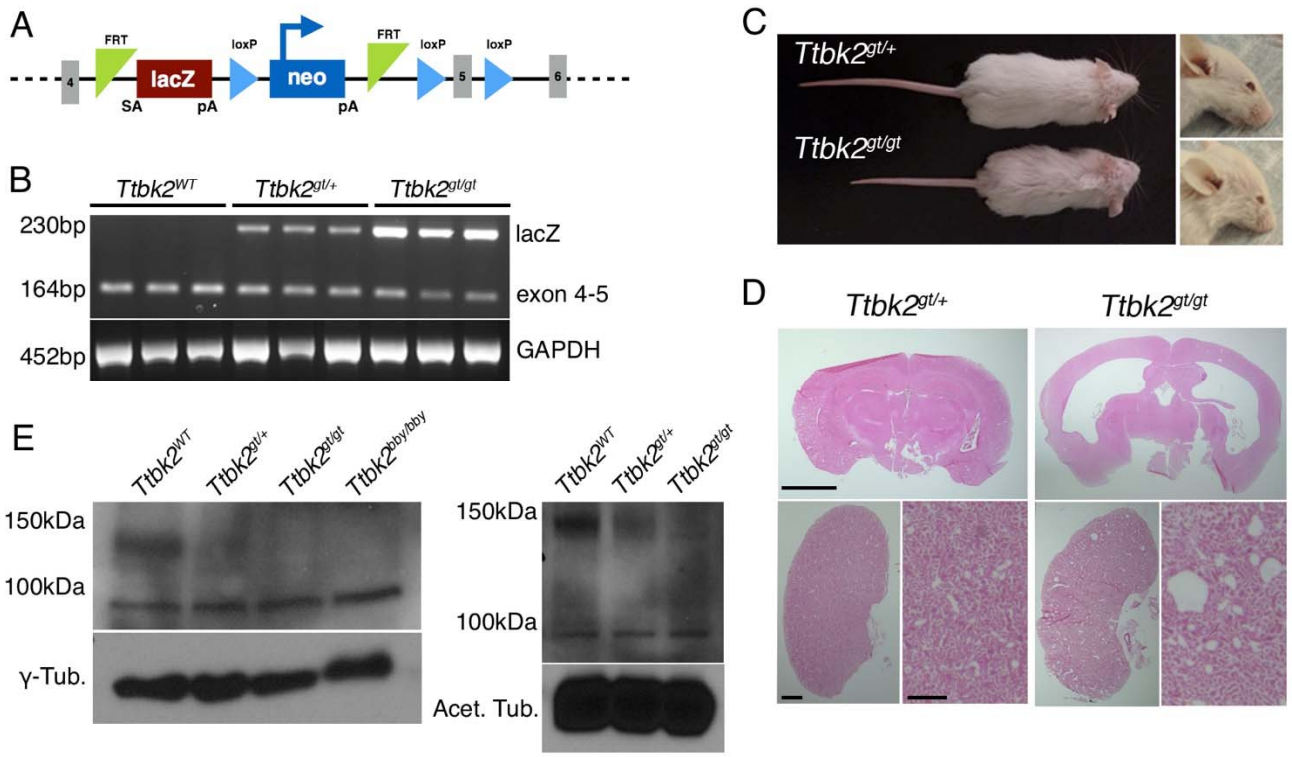

Figure S3

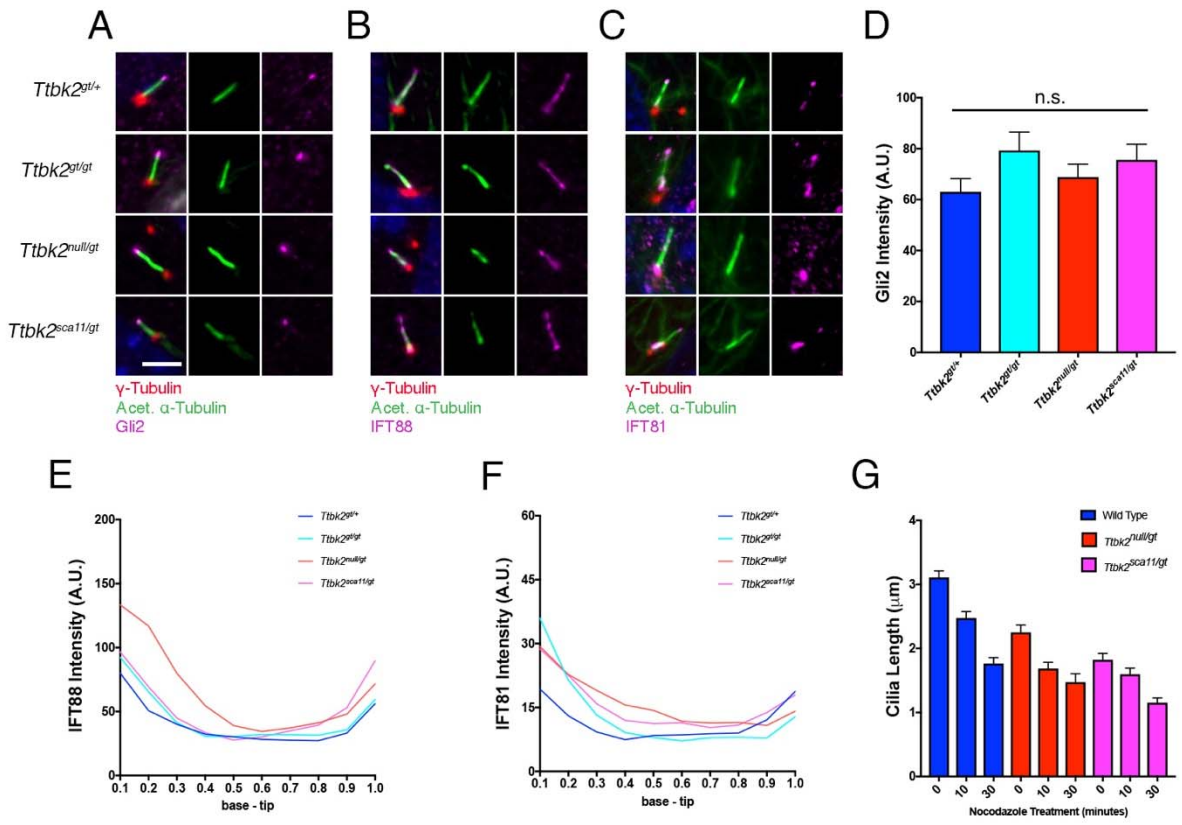

Figure S4